LIDAR MAPPING SUPPORTING EARTHQUAKE RESEARCH OF THE SAN ANDREAS FAULT

Charles Toth[1], Dorota Brzezinska[2], Nora Csanyi[1], Eva Paska[1] and Naci Yastikli[3]
[1]Center for Mapping
[2]Department of Civil and Environmental Engineering and Geodetic Science
The Ohio State University
Columbus, OH 43212
[3]Department of Geodetic and Photogrammetric Engineering
Yildiz Technical University
toth@cfm.ohio-state.edu

ABSTRACT

To support earthquake research, a dedicated LiDAR survey was conducted to map an approximately 1,000 km segment of the San Andreas and San Jacinto Faults in southern California in the spring of 2005. The Ohio State University-led team included NCALM from University of Florida, USGS, Navtec and Optech International. The project was funded by the National Science Foundation, and the primary objective was to create a highly accurate DEM along the fault line before the Big One happens. To achieve the highest possible accuracy, extreme care was devoted to all of the system components and to the mission planning of the LiDAR survey. A dense network of GPS reference stations was established in addition to the POB system to provide short baselines for the sensor platform orientation. For QA/QC purposes, conventional profiles were surveyed and LiDAR-specific targets were used. These targets provided not only for vertical correction but were able to assess the horizontal accuracy (relative to the laser pulse footprint size). The paper provides a project overview and an analysis of the achieved accuracy.

INTRODUCTION

The project B4, codenamed to reference to the "before" status of a widely anticipated major earthquake, the Big One, is a National Science Foundation (NSF) sponsored project, led by scientists from The Ohio State University (OSU) and the U.S. Geological Surveys (USGS), to create an unprecedentedly accurate surface model (DEM) along the San Andreas and San Jacinto Faults in southern California. Besides the USGS, the OSU-led team included NCALM (National Center for Airborne Laser Mapping) from the University of Florida, UNAVCO (a non-profit, membership-governed consortium, supporting Earth science) and Optech International.

The team completed an Airborne Laser Swath Mapping (ALSM) survey of ~1,000 km of the southern San Andreas Fault and San Jacinto Fault systems in May 2005. The main objectives of this project were: (1) to capture in great detail the topography of the near-field of these faults prior to the Big One, so that after a great earthquake occurs the survey can be repeated to examine the near-field displacements (coseismic and postseismic) in extraordinary detail, and thereby resolve some of the great debates about earthquake source physics, (2) provide our present results to geomorphologists and paleoseismologists, who can use offsets in topography to address the history of major earthquakes along these faults, and to guide the selection of new trenching sites and dating, and (3) improve the near-field geodetic infrastructure of these fault systems. Large numbers of volunteers played a crucial role in the original field measurements, and the indications are that the group of science data users will continue to grow as we move from raw data, through preliminary data products, to the refined and higher level data products.

B4 PROJECT AREA AND AIRBORNE SURVEYS

The project aimed to investigate the primary continental transform fault of the North American – Pacific plate boundary, the southern San Andreas fault (SSAF), see Figure 1, from just northwest of Parkfield to Bombay Beach, California (e.g., Wallace, 1949 and 1990; Matti and Morton, 1993). This section of the fault includes the transition from creeping to locked zones along-strike at the northwestern end, as well as what is known as the Big Bend and

both tectonic 'knots' at Tejon Pass and San Gorgonio Pass (e.g., Sykes and Seeber, 1985). Furthermore, it includes perhaps the most heavily primed section of the entire San Andreas Fault that runs down the Coachella Valley to its southeastern terminus at Durmid Hill. Of the many possible "Big Ones" on the southern San Andreas Fault, the acquired dataset is likely to cover them all. If the pre-event imagery obtained by this study were to be differenced with post-event imagery, an unprecedented mapping of the near-fault pattern of deformation would result in a very high-resolution, three-dimensional displacement field along the entire rupture zone.

From Cajon Pass towards the southeast to Whitewater is a section that remains highly controversial, since some investigators believe it has accumulated as much as 14 meters of slip since the last event, whereas others feel that it may have slipped as recently as 1812 or 1857 and hence has little accumulated strain (e.g., McGill and Rubin, 1999). The San Bernardino Mountains to the north, and San Jacinto Mountains to the south, press together across the multiple traces of the San Andreas Fault zone. Some 10-15 mm/yr of right-lateral shear strain makes its way around the east end of the Big Bend, from the San Andreas fault in the Coachella Valley (near Indio and Palm Springs) to the Eastern California Shear Zone (ECSZ; near Yucca Valley and Landers). A similar amount may feed from the San Jacinto Fault to the Mojave segment of the San Andreas Fault (to the northwest of Cajon Pass). The amount of strain occurring within this complex portion is not clear, but may be as little as 5 mm/yr or as much as 15 mm/yr. Recent studies of the Coachella Valley segment confirm that several hundred years have elapsed while the fault continues to accumulate strain at a high rate (e.g., Fumal *et.al.*, 1993), clearly indicative of a strong proclivity toward future seismic rupture.

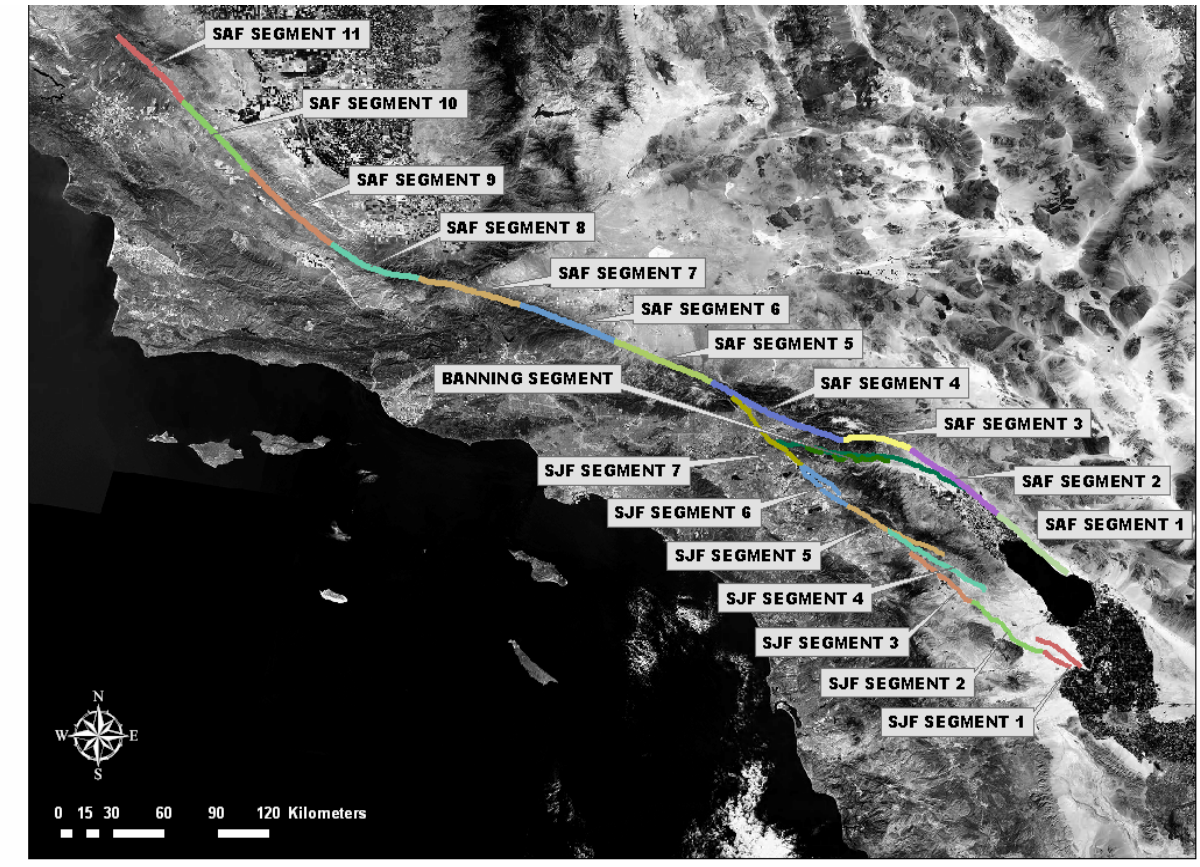

Figure 1. The southern San Andreas and San Jacinto Faults; segments show about 50 km sections of the fault lines that were flown over 5-6 times with 50% overlap in a single mission.

The airborne surveys took place May 15-25, 2005. A Cessna 310 aircraft was hired and Optech International provided the ALTM 3100 system at no cost to the project. NCALM was in the charge of the flight operations. OSU was the lead team for the GPS work, which was assisted by UNAVCO and USGS Pasadena staff. The ground LiDAR target and profiling operations were supported by two OSU field teams.
The airborne sensor suite included:

- The state-of-the-art Optech 3100 system configured for 70 kHz pulse rate. This represented an optimal balance between the high spatial resolution of the LiDAR points and a good accuracy for the range measurements.
- In addition to the built-in Applanix POS component of the Optech 3100 system, a Honeywell H764G IMU unit was also installed in the airplane. The increased redundancy offered a potential for improved QA/QC processes, as well as for better combined georeferencing results.
- An experimental color-infrared digital camera was installed next to the Optech 3100 system, providing imagery of 1K by 2K resolution in four bands; images were captured at 1 Hz, synchronized to the 1PPS GPS signal.

The project area, encompassing about 1,000 km of fault line, was segmented into smaller sections during flight planning, including the San Andreas and San Jacinto Fault lines (SAF and SJF) as shown in Figure 1. Each segment was about 50 km long and to achieve a swath width of about 1,000 m with double LiDAR coverage, 5-6 flight lines with 50% overlap were flown. On a typical day, two segments were mapped, each requiring about a net 2 hours of sensor-on time.

To achieve the highest possible georeferencing performance of the airborne platform, a dense network of GPS reference stations was established along the fault line. About 100 new stations were set up at an average spacing of 10 km. These stations were occupied for about 6-10 hours to support the LiDAR flights, as well as to allow for referencing them to the POB system; the POB reference stations close to the fault lines were also switched to a 1 Hz data acquisition rate for the duration of the data acquisition campaign.

For QA/QC of the LiDAR points, as well as for the additional strip corrections, mobile LiDAR-specific targets were used throughout the surveys. Typically, two clusters of 3-4 targets were evenly placed along the approximately 50 km long flight segments. The target cluster location was planned to be located at around 1/3 and 2/3 of the segment length. However, due to access difficulties, such as excessive drive time or lack of drivable roads, the actual location varied on a wider scale.

DATA PROCESSING

The ten days of intense airborne and ground surveys produced a massive amount of data, presenting a rather complex and time-consuming data processing task for the team. First, the GPS reference station network was processed. Subsequently, based on those results, the flight lines were processed, followed by the creation of the initial LiDAR point datasets to meet the delivery of a preliminary product, urgently expected by the earthquake research community. In the second phase, refinements are being applied in every stage of the processing to achieve the highest possible accuracy of the end products. This process is still going on and final results are expected later this year. In the following, a few samples are shown to indicate important aspects, and an initial accuracy analysis of the data processing.

The GPS reference station network adjustment was performed at OSU. The GAMIT software was used for this processing task. Initial results were made available in July, 2005, and the final results were released in October, 2005. The accuracy of the second adjustment resulted in about 3 mm horizontal and 10 mm vertical accuracy, see (Bevis *et.al*., 2005).

The flight lines were initially processed by the KARS software (Mader, 1992), and the results were used to merge with the Applanix IMU data to provide the sensor orientation for the LiDAR system. To achieve high reliability of the GPS flight line results, two independent groups performed a thorough analysis of select flight line solutions with respect to the base stations used. The objective of the comparative investigation was to decide whether to use double differenced L1 phase solution or L3, ionosphere free solution, and to formulate a method for how to utilize the available base stations along the flight lines for the most accurate solution. Furthermore, the comparison of the solutions computed with different base stations along the flight lines confirmed an about 1-2 cm accuracy of the base station coordinates. To compute the final trajectory from the overlapping solutions with the different base stations, a weighted average was calculated with the weights based on the RMS values of the individual solutions. Due to high redundancy, this method provides a superior solution compared to methods using only one base station, and thereby can provide improved accuracy of the final LiDAR product. Details on the flight line processing and the selected strategies are found (Toth et.al, 2006; and Csanyi et.al., 2007).

The initial level-one LiDAR product was created by NCLAM and released to the scientific community in two parts in 2006 (Hudnut, 2006).

QA/QC ANALYSIS

To ensure the highest possible accuracy of the final B4 DEM product, after the initial release of the B4 data, all the input datasets and processing techniques were carefully analyzed, so depending on findings, a refined product could be created and ultimately released in the future. The GPS processing, obviously, is finished, but due to strong dependency of the different data processing phases on the results of other processing steps, this ongoing investigation is expected to be completed in 2007.

LiDAR Product Characterization by LiDAR-specific Ground Control

The LiDAR-specific targets deployed in the project area for the airborne surveys represent the only independent means of validating the accuracy of the surface points, as there are very few man-made features along the San Andreas Fault that could be used for absolute quality control. During the B4 flights, two ground control teams, each using four LiDAR-specific targets, placed a cluster of targets in the middle of the surveyed swaths, with even spacing along each fault segment. A target specifically designed for the B4 project (the LiDAR target concept and prototype were developed earlier for ODOT, see Toth and Brzezinska, 2005), shown with approximate dimensions in Figure 2, could provide good vertical control from about 1-2 pts/m^2 LiDAR point density. The double concentric circle design with different coating allows for improved horizontal control provided the LiDAR point density is at least 4 pts/m^2 (at the given target size).

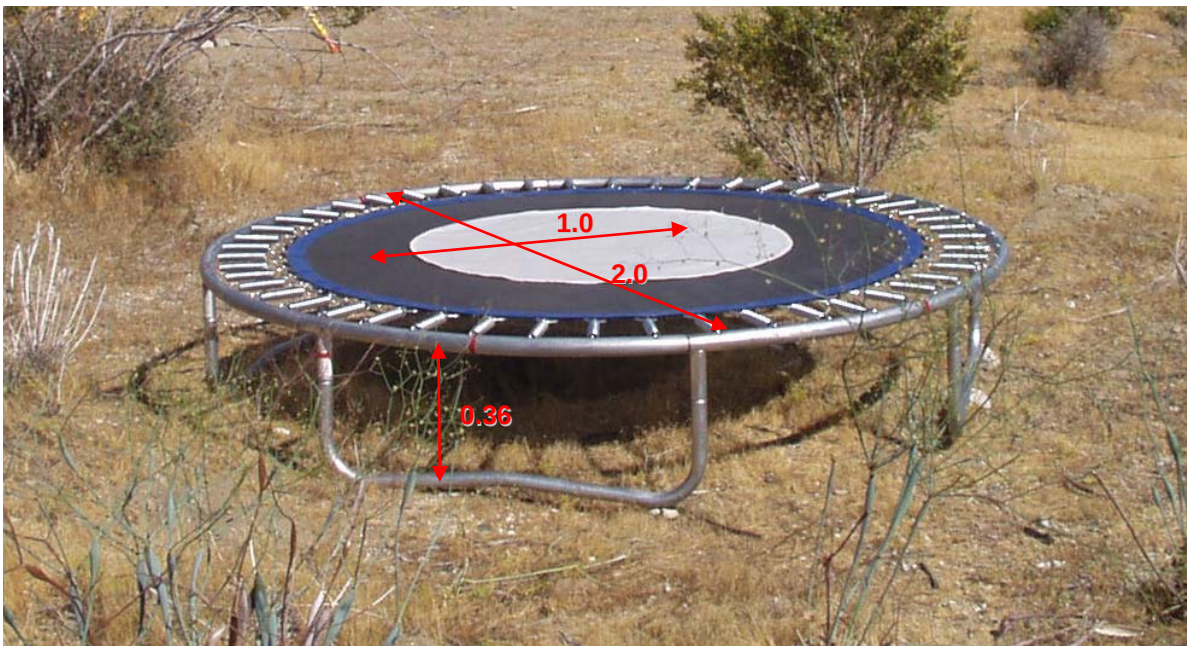

Figure 2. LiDAR-specific ground target specifically developed for the B4 project.

The LiDAR targets were GPS surveyed during deployment, including six observations along the perimeter ring of the target. Using the closest GPS base station, the NGS KARS software (Mader, 1992) was used to determine the location of the target, and then the coordinates of the center of the target were determined at accuracy (1σ) of 1 cm and 2 cm horizontally and vertically, respectively. By comparing the coordinates of the LiDAR-determined target positions to the target GPS-surveyed coordinates, the accuracy of LiDAR point cloud can be assessed. Depending on target distribution and observed differences, if needed, corrections can be applied to the LiDAR point cloud to improve the accuracy of the data set. A fully-automated method was developed to determine the target location from the LiDAR points fallen on targets, including the filtering of the points reflected back from targets and the estimation of the position of the center of the target. The details of these procedures can be found in (Csanyi et al, 2005; Csanyi and Toth, 2007).

Table 1 shows the summary of the results of comparing the GPS-surveyed target control coordinates to the LiDAR-determined target positions, organized according to the fault segments in the order as they were acquired.

The LiDAR data used in this analysis is the NCALM-produced level-one point cloud. During the B4 project, a segment was on average flown five times with 50% overlap and consequently a single target normally appeared in 2-3 flight lines. The overall LiDAR point density realized in the B4 project was 2 pts/m^2 and provided an excellent vertical component analysis, while the horizontal accuracy could be checked only at a rather coarse level. Table 1 shows the mean, the RMSE and the maximum errors for each flight segment. The number of targets used for full or for vertical-only comparisons are also listed, indicating that the analysis of the horizontal component was feasible only for about half of the targets.

Table 1. LiDAR point errors at target locations.

	Mean error [m]			RMSE [m]			Max error [m]			No. of targets	
Segment	**E**	**N**	**height**	**E**	**N**	**height**	**E**	**N**	**height**	**XYZ**	**Z**
SAF11	0.05	-0.13	0.04	0.16	0.15	0.05	0.29	0.2	0.08	4	8
SAF10	-0.14	-0.4	0.01	0.14	0.40	0.03	0.14	0.4	0.05	1	5
SAF09	-0.14	-0.43	-0.01	0.14	0.43	0.03	0.14	0.43	0.05	1	3
SAF08			0.01			0.01			0.01		1
SAF07	-0.01	-0.17	0.00	0.01	0.17	0.02	0.01	0.17	0.04	1	3
SAF06	0.06	-0.25	-0.01	0.06	0.25	0.00	0.06	0.25	0.00	1	2
SAF05	0.09	-0.2	0.12	0.17	0.22	0.13	0.24	0.30	0.18	3	4
SAF04	-0.06	-0.27	-0.03	0.07	0.32	0.04	0.10	0.45	0.06	2	3
SAF03	-0.08	-0.05	0.17	0.08	0.08	0.18	0.11	0.11	0.26	2	5
SAF02											
SAF01	0.15	-0.17	0.00	0.16	0.18	0.03	0.21	0.23	0.04	3	6
SJF01	0.05	-0.26	0.16	0.07	0.28	0.16	0.10	0.36	0.19	2	4
SJF02	-0.04	-0.31	-0.02	0.09	0.34	0.06	0.14	0.50	0.09	3	5
SJF03											
SJF04											
SJF05	-0.08	-0.22	-0.02	0.11	0.31	0.06	0.16	0.46	0.12	9	12
SJF06	-0.05	-0.14	-0.01	0.13	0.17	0.03	0.21	0.27	0.06	4	5
SJF07											
Banning1	0.17	-0.05	-0.08	0.17	0.05	0.09	0.17	0.05	0.13	1	4
Ban. 2,3,4	-0.01	-0.23	0.00	0.13	0.39	0.11	0.2	0.62	0.18	9	12
Mean	**0.00**	**-0.22**	**0.02**	**0.11**	**0.25**	**0.06**	**0.29**	**0.46**	**0.26**	**46**	**83**

There were about 7.5 billion LiDAR points measured in the B4 project and only about 500 points fell on the LiDAR-specific targets. Nevertheless, the points reflected back from the targets were rather evenly distributed in space (and in time), and thus the analysis of the observed differences provides a statistically meaningful quality assessment for the LiDAR product. Looking at the cumulative results, the mean of the height differences is 2 cm, which is a good value and indicates negligible bias in the data in the vertical direction, and the RMSE of the difference, averaged by segments, is 6 cm, an excellent accuracy with respect to typical airborne LiDAR surveying results; both parameters indicate geodetic quality LiDAR in the vertical direction. The horizontal accuracy values are larger, as expected, yet they should be considered good, since they are less than the LiDAR footprint size, which was about 25 cm on average for the average flight altitude.

The vertical accuracy assessment of the LiDAR data set was done according to the ASPRS LiDAR Guidelines, see also in (Maune, 2007); the B4 project met the ASPRS QA/QC checkpoint requirements:

- The ASPRS Guidelines require the checkpoints to be selected on flat terrain or on uniformly sloping terrain. This requirement was satisfied, since during the surveys the LiDAR-specific targets were placed on near horizontal open terrain.
- The QA/QC surveys should be such that the checkpoint accuracy is at least three times better than the accuracy of the dataset being evaluated. This requirement was satisfied since the targets were GPS-surveyed with an about 1 cm horizontal and 1-2 cm vertical accuracy, which is more than three times better than the expected LiDAR data accuracy.
- The guidelines recommend utilizing a minimum of 20 checkpoints in the project area. This recommendation was satisfied during the LiDAR survey, since 83 LiDAR targets were successfully identified in the project area.
- In all methods of accuracy testing and reporting, there is a presumption that the checkpoint surveys are error free and the discrepancies are attributable to the remote sensing technology assumed to have lower accuracy.

The LiDAR targets were placed on open terrain, and therefore, the Fundamental Vertical Accuracy calculation method should be applied. To check whether the actual errors can indeed be considered normally distributed and to check for any blunders in the errors, the histogram of the errors was assessed and the skewness value, as an indicator of how well the errors can be considered normally distributed, was computed. The histogram and computed statistics are shown in Figure 3 and Table 2 (83 targets).

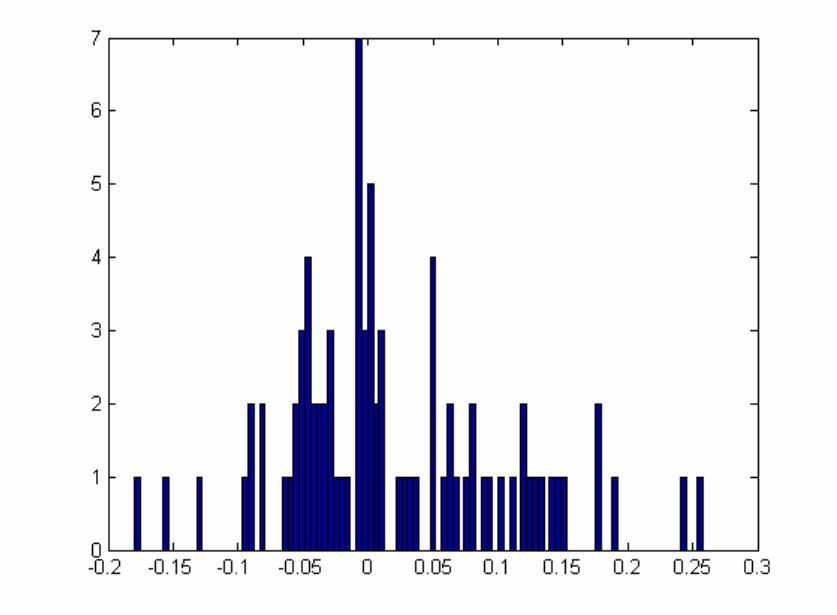

Figure 3. Histogram of errors measured at the LiDAR targets.

Table 2. Statistical parameters of the error distribution.

No. of targets	$RMSE_z$ [m]	Std [m]	Skewness
83	0.09	0.08	0.55
81	0.08	0.08	0.28

The guidelines state that a dataset can be considered normally distributed if the skewness value does not exceed ±0.5. The computed skewness value 0.55 exceeds this threshold, which indicates that the errors are only close to being normally distributed. By looking at the histogram, it is obvious that the histogram is skewed to the right by two values that might be outliers. A generally accepted rule is that a potential blunder may be identified as any error greater than three times the standard deviation (3σ) of the error. Based on this rule, two of the found errors (with values of 0.24 and 0.26 m) were considered as blunders, and consequently were removed from the dataset for the final accuracy assessment calculations; the recomputed statistical parameters are shown in Table 2 (81 targets).
As the 0.28 skewness value indicates, the vertical errors can be considered normally distributed, and therefore, according to the ASPRS Guidelines, the vertical accuracy of the B4 dataset is 15 cm (1.96 x RMSE) at the 95% confidence level. Another widely used accuracy term is the RMSE which is 8 cm for the B4 dataset.

LiDAR Product Characterization by Ground Profile Control

Short ground profiles were GPS-measured around the LiDAR-specific targets for providing additional ground control to support the LiDAR product validation. Using a helmet-mounted GPS antenna, the surveying crew in charge of the LiDAR targets walked in the vicinity of the targets, measuring profiles in the direction perpendicular to the flight lines (wherever it was possible). In contrast to the targets, the profiles provide ground control in a significantly larger spatial context. However, the use of profiles in general poses more challenges, as it is more complicated to compare the two data entities. Both datasets, the LiDAR point cloud and the profile GPS points, come with irregular point distribution, and the LiDAR data have rather sizeable horizontal uncertainty, plus the profile data are subject to human dynamics motion of the operator, all making the interpolation of the data difficult and limiting the accuracy of the comparisons. About 80% of the collected profiles were successfully processed, i.e., good quality survey profiles were computed by the KARS software and thus could be used for comparisons, which are expected to be released later this year.

Comparative Analysis of the Two GPS/IMU Georeferencing Systems

Airborne LiDAR systems are based on direct georeferencing, and consequently the achieved accuracy of the platform position and attitude is of utmost interest, as it sets the lower bound for the error budget (additional terms include the laser ranging error, sensor calibration and object characteristics). Currently, integrated GPS/IMU sensors represent the state-of-the-art in airborne georeferencing and can deliver cm-level positioning and 20-30 arcsec attitude accuracy under favorable conditions (e. g., Skaloud et al., 1996; Mostafa et al., 1998; Grejner-Brzezinska, 1999). The Optech ALTM 3100 LiDAR has a built-in GPS/IMU positioning system from Applanix (http://www.applanix.com/products/pospac_airborne_index.php). The installation of a second georeferencing system next to the LiDAR sensor in the B4 project had several advantages, as it could provide data redundancy and facilitate various independent testing, especially if the second system provides an access to raw data. Since there are only negligible differences in the performance of geodetic grade receivers, the duplication of the IMU, in particular with the OSU-owned Honeywell H764G higher-grade sensor, was satisfactory for the B4 project (due to last minute changes in the aircraft hardware, unfortunately, the H764G IMU could not been placed next to the laser sensor).

For comparative analysis, the navigation solutions were obtained by the Applanix POSPac and the AIMS software (e.g., Grejner-Brzezinska et al., 1998); both used the Applanix POSGPS solution, and are based on the implementation of an Extended Kalman Filter (EKF), although they use different state variables. The accuracy assessments of an EKF solution are known to be overly optimistic, and therefore, the comparison between the two navigation solutions provided a rare opportunity for a better assessment of the estimated parameter accuracies. Table 3 lists the EKF estimated results for both solutions as well as the difference between the two solutions based on a typical B4 flight.

Table 3. RMS error of navigation solutions for flight line 147_23 and accuracy terms (std) obtained from the parameters' differences.

	Error terms					
	Position			Attitude		
	X [m]	Y [m]	Z [m]	ω [‘]	φ [‘]	κ [‘]
POSPac solution	0.02	0.02	0.3	0.25	0.24	1.53
AIMS solution	0.01	0.01	0.2	0.05	0.05	0.1
Differences	**0.02**	**0.02**	**0.03**	**0.70**	**0.60**	**1.07**

Analyzing the results, the estimated positioning performance clearly shows a reasonably good match, as expected. It is also visible that the AIMS attitude estimations could be somewhat optimistic, even assuming that the specs for the high-end H764G are about an order better than that of the DMARS-I IMU. Of particular interest are the attitude angle differences between the two navigation solutions, where a noticeable difference exists. This can be explained by the above mentioned underestimation of the terms in the EKF in AIMS and/or by possible flexing between the two sensors (the OSU H764G was installed about 1 m away from the Applanix IMU; both were attached to the floor of the airplane). In the roll and pitch components, the differences are significantly higher than expected and thus both phenomena could have contributed to these increased values. The heading, in comparison, shows a smaller value than expected, and that may indicate that the Applanix heading error estimate is slightly pessimistic. Given the aircraft structure and the placement of the two IMU sensors, mechanical flexing have had no or negligible impact on heading.

Obviously, no absolute check was feasible in this case as the B4 imagery was not good enough for highly-accurate positioning, and thus, only internal consistency checks between the two IMU sensors could be performed. Another way to interpret the data is to accept the accuracy terms for the difference and deduct backward what the realistic accuracy terms could have been for the solutions, and then check their validity by using the imaging sensor positioning results. This approach results in a good match with the accuracy analysis of the LiDAR targets. The impact of the roll and pitch components produce a vertical error nearly proportional to the scan angle and would account for a maximum vertical error of about 2 cm. The heading term would impact only the horizontal accuracy, which can be about maximum 5 cm (proportional to the scan angle). In summary, the 2 cm vertical impact is far smaller than the mean error or the 95% CEP accuracy qualification of the LiDAR product.

Further investigations will address the impact of longer flight lines when the heading component should experience a growing error, and thus the performance difference between two IMUs could be significant, which is not the case for shorter flight lines in good GPS availability conditions (open-sky).

Evaluation of the B4 Imagery

The primary focus of the B4 project was to acquire a highly-accurate topographic description of all the geological features along the southern California San Andreas and Jacinto Fault lines. Clearly, a carefully planned and executed airborne LiDAR survey can provide this type of information. However, human operators are very used to visual information, and therefore a visual coverage along the fault lines was highly desirable; LiDAR is in a way a "blind" sensor, as it provides intensity information only in a narrow band of the visible and near-IR spectrum. In addition, having high-resolution, metric quality image data could be used to improve the topographic description of the fault lines as it can provide spatial information besides the radiometric data. Unfortunately, no high-performance airborne digital camera was available and the B4 project was flown with the experimental NCLAM camera.

The NCLAM-owned RedLake MS4100-RGB camera is a general-purpose industrial camera, providing moderate image resolution, 2K by 1K, with true four-band multispectral radiometric capabilities (4 CCD design). In addition, the camera can operate with high data capture rate compared to the usual airborne digital cameras. The camera triggering was synchronized to the 1PPS GPS signal and consequently images were acquired at every second; about half the B4 project was imaged during the airborne surveys. The camera was configured to capture imagery in CIR mode. To better assess the capabilities of the NCALM RedLake camera, Table 4 shows a parameter comparison to a mainstream airborne digital camera (Intergraph DMC).

Table 4. Parameter comparison of the RedLake and DMC cameras.

	RedLake MS4100-RGB	Z/I DMC
Image size	1,920 x 1,080	13,824 x 7,680
Pixel size [μm]	7.4	12
Intensity [bit]	8	12
Focal length [mm]	26	120
FOV [°]	30.6 x 17.5	69.3 x 42
GSD [cm] at 800 m AGL	23	8
Capture rate [FPS]	4	1
Pan/Multispectral bands	0+4	4 + 4

To extract accurate geospatial data (position of objects) from an imaging sensor, the camera must be calibrated and boresighted to the georeferencing sensors. NCALM arranged for a calibration of the camera at the USGS EROS digital camera calibration facility in Sioux Falls prior to the flights. The USGS camera calibration report shows typical parameters in general, and there was only one really critical comment in the report, stating that the CCD chips could move within about 4 pixels. The boresight calibration had to be based on the B4 dataset, as the camera was installed in the field, and thus there was no specific boresight test flight done to determine the boresight calibration parameters. The release of the first batch of the NCALM LiDAR dataset offered the first opportunity to perform an aerial triangulation and consequently determine the boresight parameters. An area rich in man-made features was selected and using the LiDAR range and intensity data, ground control points were created. These points had rather modest accuracy, as described above in the LiDAR product characterization, yet using a large number of points could partially compensate for the low accuracy for our purpose. The triangulation results, as expected, were far below the usual values obtained by large-format aerial cameras in comparable flight conditions. Using the theoretical error estimate formulas for stereo models (Kraus, 1993), the vertical accuracy term for an object point extracted from stereo images can be estimated for the B4 imagery as:

$$\sigma_z = \frac{Z}{c} \cdot \frac{Z}{B} \cdot \sigma_p = \frac{800}{0.026} \cdot \frac{800}{50} \cdot 0.000007 = 3.44 \text{ [m]}$$

Where $\boldsymbol{Z}$ stands for the flying height (AGL), $\boldsymbol{B}$ for the base, $\boldsymbol{c}$ is the camera constant, and is $\boldsymbol{\sigma_p}$ the parallax measuring accuracy. Clearly, the rather large error term is mainly due to the small image scale (Z/c) and to the extreme base/height (B/Z) ratio, 0.06 for the B4 imagery, which is an order smaller than the preferred 0.6 value. Applying the boresight parameters to the GPS/IMU navigation solution, the EO was computed for a block of images. Using conventional ray intersection, the feature positioning accuracy of the stereo models was assessed. Table 5 shows the results for the test block.

Table 5. Positioning results with direct georeferencing.

Control / Check Points	**σ_0 [μ]**	**RMS at Check Points [m]**		
		X	**Y**	**Z**
0 / 25	**46**	**1.18**	**0.70**	**5.57**

The residuals look rather large in comparison to the aerial triangulation results. However, the direct georeferencing has a different error model (extrapolation) and is sensitive to sensor calibration, thus the larger RMS values are justified. Given the general image quality of the RedLake camera in the B4 airborne survey conditions, including geometric and radiometric behavior, the B4 imagery does not allow for accurate map production and can only be used for visualization.

CONCLUSION

The B4 Project Team performed a high-resolution topographic survey of the San Andreas and San Jacinto fault zones in southern California, in order to obtain pre-earthquake imagery necessary to determine near-field ground deformation after a future large event and to support tectonic and paleoseismic research. The B4 project to map the topography along the fault lines at unprecedented accuracy has produced excellent initial results. The dense GPS reference network, combined with meticulous processing, resulted in very accurate flight line trajectories, and consequently provided an exceptionally small navigation error budget for the airborne platform. The excellent ranging accuracy of the LiDAR sensor, combined with the high-quality navigation solution resulted in a vertical LiDAR point accuracy falling in the sub-decimeter range and can be further improved where ground control is available. The complete B4 dataset will be archived at the NCALM Berkeley web-site and the GEON portal.

ACKNOWLEDGEMENTS

The B4 project was funded by the National Science Foundation and the ALTM 3100 system was generously provided by Optech International. The authors wish to acknowledge the support from the National Science Foundation and the contribution of many researchers from OSU, USGS, NCALM, UNAVCO and Optech International who participated in the B4 mapping project, as well as, the many OSU students who did much of the GPS observations.

REFERENCES

Bevis, M. et.al., (2005). The B4 Project: Scanning the San Andreas and San Jacinto Fault Zones, Eos Trans. AGU, 86(52), Fall Meet. Suppl., H34B-01.

Csanyi, N., C. Toth, D. Grejner-Brzezinska and J. Ray (2005). Improving LiDAR data accuracy using LiDAR-specific ground targets, ASPRS Annual Conference, Baltimore, MD, March 7-11, CD-ROM.

Csanyi, N. and C. Toth (2006). Improvement of LiDAR Data Accuracy Using LiDAR-Specific Ground Targets, *Photogrammetric Engineering & Remote Sensing*, Vol. 73, No. 5.

Csanyi, N., K. Edwards, D, Brzezinska and C. Toth (2007). Geodetic Grade Airborne LiDAR Mapping, ION NTM 2007, San Diego, CA, January 22-24, CD-ROM.

Fumal, T.E., S.K. Pezzopane, R.J. Weldon and D.P. Schwartz (1993). A 100-year average recurrence interval for the San Andreas Fault at Wrightwood, California: *Science*, v. 259, p. 199-203.

Grejner-Brzezinska D. A., (1999). Direct Exterior Orientation of Airborne Imagery with GPS/INS System: *Performance Analysis, Navigation*, Vol. 46, No. 4, pp. 261-270.

Grejner-Brzezinska D. A., R. Da and C. Toth (1998): GPS Error Modeling and OTF Ambiguity Resolution for High-Accuracy GPS/INS Integrated System, *Journal of Geodesy*, 72(11), pp. 628-638.

Hudnut, K., (2006). The San Andreas Fault: Exposed!, USGS Lecture Series, Pasadena, CA, November 3, 2006.

Kraus, K., (1993). *Photogrammetry Volume I*, Dummler Books.

Mader, G.L., 1(992). Rapid Static and Kinematic Global Positioning System Solutions Using the Ambiguity Function Technique, *Journal of Geophysical Research*, 97, 3271-3283.

Matti, J.C. and D.M. Morton (1993). Paleogeographic evolution of the San Andreas fault in southern California: a reconstruction based on a new cross-fault correlation, in Powell, R.E., Weldon, R.J., and Matti, J.C., eds., *The San Andreas fault system: displacement, palinspastic reconstruction, and geologic evolution*: Geological Society of America Memoir 178, p. 107-159.

McGill, S. F. and C. M. Rubin (1999). Surficial slip distribution on the central Emerson fault during the June 28, 1992, Landers earthquake, California, J. Geophys. *Res*., vol. 104, #B3, pp. 4811-4833.

Maune, D., (2007). Digital Elevation Model Technologies and Applications: *The DEM Users Manual, 2nd Edition*, ASPRS.

Mostafa M. M., K.P. Schwarz, and M.A. Chapman (1998). Development and Testing of an Airborne Remote Sensing Multi-Sensor System, ISPRS COMM. II Symposium on Data Integration: Systems and Techniques, July 13-17, 1998, Cambridge, England, pp.217-222.

Sykes, L.R. and L. Seeber (1985). Great earthquakes and great asperities, San Andreas fault, southern California: *Geology*, v. 13, no. 12, p. 835-838.

Skaloud, J., M. Cramer, and K.P. Schwarz (1996). Exterior Orientation by Direct Measurement of Camera Position andAttitude, *International Archives of Photogrammetry and Remote Sensing*, Vol. XXXI, Part B3, 1996, pp. 125-130.

Toth, Ch. and D. Brzezinska (2005). Geo-Referenced Digital Data Acquisition and Processing System Using LIDAR Technology, ODOT Report No. 14799, 2005.

Toth, C. K., D. Grejner-Brzezinska and M. Bevis (2006). Extreme Precision LiDAR Mapping, From Sensors to Imagery, ISPRS Commission I Symposium, Paris, France, July 4-6.

Wallace, R.E., ed., (1990). The San Andreas Fault system, California: U.S. Geological Survey Professional Paper 1515, 283 p.

Wallace, R.E., (1949). Structure of a portion of the San Andreas rift in southern California: *Geological Society of America Bulletin*, v. 60, no. 4, p. 781-806.